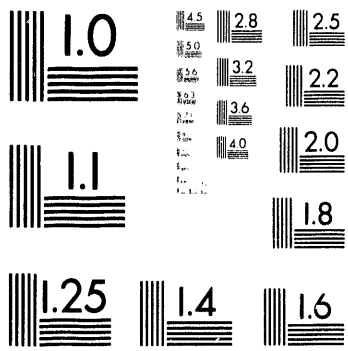
1.0
1.1
1.25
1.4
1.6
1.8
2.0
2.2
2.5
2.8
3.2
3.6
4.0
4.5
5.0
5.6

1 of 1

Conf-9401103--1

VERTICAL-TUBE AQUEOUS LiBr FALLING FILM ABSORPTION USING ADVANCED SURFACES

William A. Miller
Horacio Perez-Blanco*

*Penn State University
University Park, Pennsylvania

To be presented at
International Absorption Heat Pump Conference
New Orleans, Louisiana
January 1994

Prepared by the
OAK RIDGE NATIONAL LABORATORY
Oak Ridge, Tennessee 37831
managed by
MARTIN MARIETTA ENERGY SYSTEMS, INC.
under Contract No. DE-AC05-84OR21400
to the
U.S. DEPARTMENT OF ENERGY
for the
Gas Research Institute

DISCLAIMER

VERTICAL-TUBE AQUEOUS LiBr FALLING FILM ABSORPTION USING ADVANCED SURFACES

William A. Miller
Energy Division
Oak Ridge National Laboratory
Oak Ridge, Tennessee

Horacio Perez-Blanco
Pennsylvania State University
University Park, Pennsylvania

ABSTRACT

A heat and mass transfer test stand was fabricated and used to investigate nonisothermal falling film absorption of water vapor into a solution of aqueous lithium bromide. The absorber was made of borosilicate glass for visual inspection of the falling film. Experiments were conducted on internally cooled tubes of about 0.019 m outside diameter and of 1.53 m length. Testing evaluated a single absorber tube's performance at varying operating conditions, namely different cooling-water flow rates, solution flow rates, pressures, temperatures, and concentrations.

Advanced surfaces were identified that enhanced absorber load and the mass of absorbed vapor. A pin-fin tube with 6.4-mm pitch absorbed about 225% more mass than did a smooth tube. A grooved tube was the second best performer with 175% enhancement over the smooth tube. Increasing the cooling water flow rate to 1.893×10^{-4} m^3/s caused about a 300% increase in the mass absorbed for the grooved tube compared with the smooth tube. Results showed that the pin-fin tube with 6.4-mm pitch and the grooved tubes may enhance absorption to levels comparable to chemical enhancement in horizontal smooth tube absorbers.

Absorber load, the transport coefficients, and pertinent absorption data are presented as functions of dimensionless numbers. These experimental data will prove useful in formulating analytical tools to predict vertical-tube absorber performance.

INTRODUCTION

It is believed that the absorption process can be enhanced with tube surfaces that induce mixing in the solution film without increasing the thickness of the film. Because the dominant concentration gradient occurs near the interface, film mixing will induce secondary flows that reduce the diffusional resistance across the film and increase mass transfer. To validate this theory, testing was conducted on a smooth tube and on several other tube geometries to determine the possible enhancements achievable through film mixing. Because the mass diffusivity of the film is low, of the order 10^{-9} m^2/s, water vapor absorbed at the interface will tend to remain at the surface unless some type of film mixing occurs. Advanced surfaces were selected with the intent of mixing the film and renewing the interface with fresh solution from the bulk of the film. Pin-fin surfaces having 26 fins per turn, a fin height of 3 mm, and three different spine pitches[1] were tested. A grooved tube surface, two twisted tube surfaces, and a fluted tube having 24 tube starts were also tested.

Laboratory testing was conducted over operating conditions that simulated field conditions for residential applications such as the DEACH system (DeVuono et al. 1990). Testing was later broadened to include commercial applications (i.e., absorber pressure of 8 mm Hg, cooling water temperature of 35 and 46°C, and concentrations of 60 through 64 wt% of LiBr brine). Testing of a smooth tube preceded testing of the advanced surfaces. Chemical additive for enhancing mass transfer had never been added to the rig prior to testing, nor was it added during the course of the experiments.

[1] Spine pitch is the longitudinal spacing between spine rows.

NOMENCLATURE

A surface area (m^2)	
ΔC,C concentration(g-mole H_2O/cc Soln)	Subscripts
D_{AB} diffusivity (m^2/s)	a absorbent LiBr brine
h enthalpy (kJ/kg)	abs absorber
K_L overall average liquid-side mass transfer coefficient (m/s)	c cooling water
$\dot{m}$ mass flow rate (kg/s)	e exit
P pressure (mm Hg)	eq equilibrium
Pr Prandtl Number [υ/α]	fg fluid-to-gas phase change
Q absorber Load (W)	flash flashed water if superheat
Re Reynolds Number $\frac{4\dot{m}}{\mu(\pi D_o)}$	i inlet
Sc Schmidt Number [υ/D_{AB}]	if interface
ΔT,T temperature (°C)	ln log-mean-difference
U overall average heat transfer coefficient $W/(m^2\text{-}K)$	l liquid-side
X concentration (wt% LiBr)	o outside tube wall
Greek Symbols	sc subcooling
μ dynamic viscosity (Kg/m-s)	v water vapor
υ kinematic viscosity (m^2/s)	
α thermal diffusivity (m^2/s)	

LABORATORY TEST STAND

The heat and mass transfer test stand is designed for testing vertical and horizontal absorbers (Fig. 1). The boiler is fired by resistance heaters of 2.5-kW capacity and generates both the water vapor and the strong solution used in the absorber. A linear gate valve trims the flow of steam to the absorber. Strong solution is pumped from the boiler and is tempered by a tube-in-tube heat exchanger to maintain saturated brine temperature as it enters the absorber. In the absorber, coupled heat and mass transfer occurs as the falling film of LiBr brine (the absorbent) absorbs water vapor (the absorbate). The film is cooled by water flowing inside the absorber tube; the flow is countercurrent to the falling film. Weak solution leaving the absorber is pumped from a sump tank and injected back into the boiler.

The absorber test section is made of standard pyrex glass pipe (i.e., 7740 borosilicate glass) 2.1 m long and 0.15 m in inside diameter (Fig. 1). A solution cup and catch basin are made of 304L stainless steel, and both are attached directly to the test tube. The cup was line bored after fabrication, and a centering collar is used to center the cup for a uniform annular gap around the test tube. Strong solution flows from the cup through the annular gap along the outer wall of the tube. The catch basin is designed for testing tubes with a maximum length of 1.53 m; however, it can be moved for testing at different absorber tube lengths. All line connections to the test absorber were fabricated from 304L stainless steel. The effect of noncondensibles was minimized through extensive leak checking using a mass spectrometer tuned for helium leak detection. Per tube tested, the test stand was certified to a leak rate of 1.0×10^{-7} atm-cc/s.

A purge tube, having ports at 0.15-m spacing over the lower 1 m of the test stand, is used to pull noncondensibles from the test section. The purge tube is connected to a nitrogen cold trap that assists a 2.4×10^{-3} m^3/s pump in pulling vacuum on the entire system. The purge tube, cold trap, and pump are also

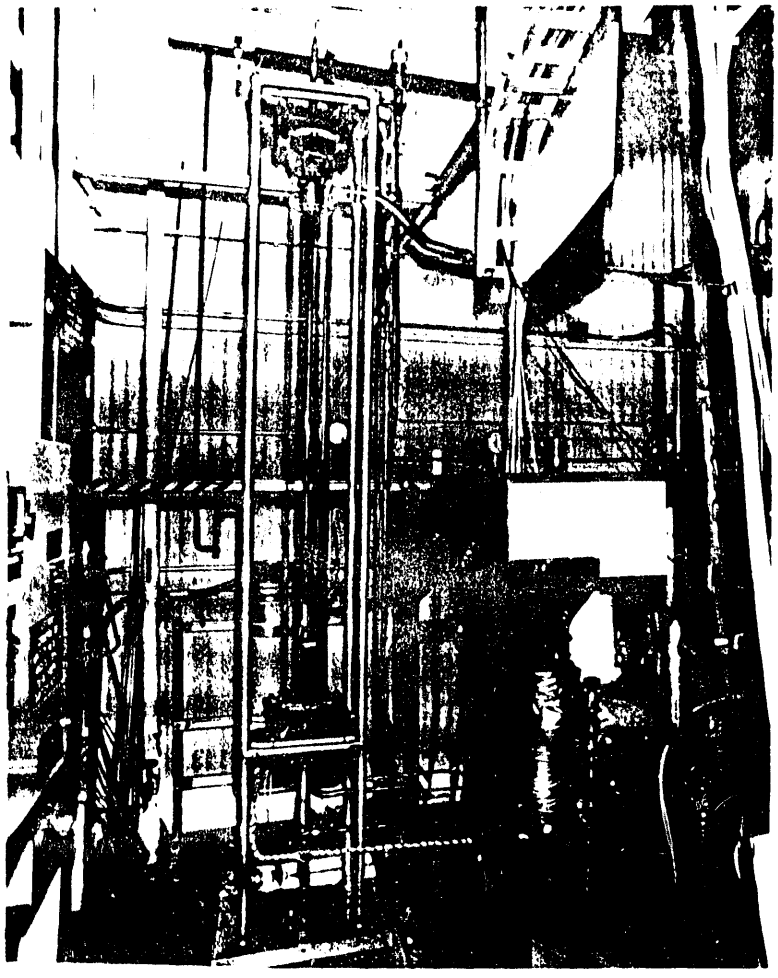

Fig. 1. PHOTOGRAPH OF LiBr-WATER ABSORBER TEST RIG.

used during absorption experiments to increase solution concentration. Water vapor is pulled from the absorber and held frozen in the cold trap. Purging of water vapor continues until the desired strong solution concentration (wt % LiBr) is obtained. This technique helps minimize crystallization dangers, especially for testing at 64 wt %. To reduce the concentration, distilled water was pulled under vacuum into the boiler and the system was operated for about 1 hour to equilibrate concentration throughout all pipe lines.

INSTRUMENTATION

Instrument locations are shown in Fig. 2. Mass flow rate and density of solution entering and leaving the absorber are measured using coriolis mass flow meters.[2] The power input to the boiler is measured using a power transducer. A turbine meter measures the cooling water flow rate. Absolute pressure transducers measure vapor pressure in the boiler and the absorber. Two temperature controllers are installed in the test stand to regulate heat to the solution lines entering and exiting the absorber to guard against potential crystallization at concentrations $\geq$ 60 wt %.

Thermocouple compression fittings are welded into each line for use in temperature measurement. A probe of 1.8-m length was inserted into the absorber test tube. It enhanced turbulent flow on the water side, and it contained thermocouples for measuring local bulk temperatures of the cooling water at 0.15-m intervals down the length of the test tube.

The setup of the two coriolis mass flow meters was altered to isolate the meters and eliminate any extraneous vibrations that could affect signal output. Previous use of a coriolis meter by Zaltash et al. (1991) showed density measurements of

[2] LiBr flows through a U-shaped tube that vibrates as a tuning fork. The transducer detects a gyroscopic force associated with moving fluid particles that is directly proportional to the mass flow rate.

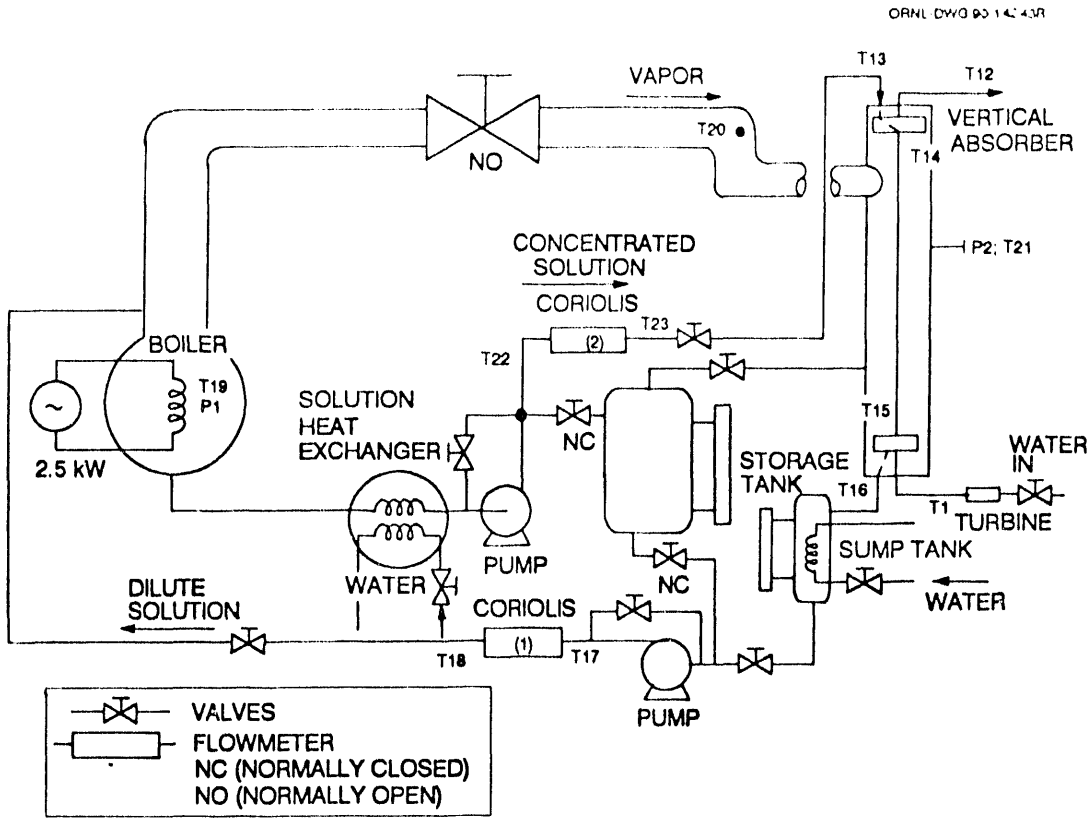

Fig. 2. SCHEMATIC OF LiBr TEST RIG.

distilled water to increase with increasing water temperature, a significant error. A similar discrepancy was found in the coriolis meters used in the LiBr-water test stand. Therefore, in-situ calibrations of the densitometers were done using various fluids of differing specific weights to verify proper density measurement. Under no-flow conditions, accuracy of measurement was better than 0.5% (i.e. ± 0.005 g/cc) for the various fluids tested. The density of distilled water was then checked as a function of temperature for nominal flows of 0.017 kg/s through the densitometers. Again, results were similar to those of Zaltash et al. (1991), tabulated data in Fig. 3, and a correction had to be made. The coriolis meters were modified by replacing the vendor's sensor, which sensed tube wall temperature, with a sensor that sensed fluid temperature leaving the meter. The modification improved instrument accuracy to about 0.5% (i.e., ± 0.006 g/cc) of reading and showed that the corrected density measurements followed the proper trend of density vs water temperature.

Samples were taken periodically to determine the concentration (wt % LiBr) of the solution, using a refractometer to measure the refractive index of the solution (Zaltash et al. 1992). Periodic checks showed in-situ measurements made with the coriolis meters to be within 0.35 wt % of sampling results. Consequently, heat balances calculated on the solution-side and the water-side were on the order of 10% in agreement.

DATA REDUCTION

As solution enters the absorber, it will be either slightly superheated or subcooled, and it will almost instantly come to equilibrium with the absorber pressure and temperature. An algorithm was developed to calculate T_{eq} at the start of the falling film. The algorithm corrects for either flashing from the film, if the solution is superheated, or the rapid mass transfer to the film, if the solution is subcooled. Using the energy equation; continuity equations; and P, X, T thermodynamic equations of state, a balance is conducted from the solution cup to the absorber inlet. Continuity yields the following relation between the solution and vapor:

$$\dot{m}_{eq} - \dot{m}_{i} = \dot{m}_{v\ abs} - \dot{m}_{v\ flash}\ , \qquad (1)$$

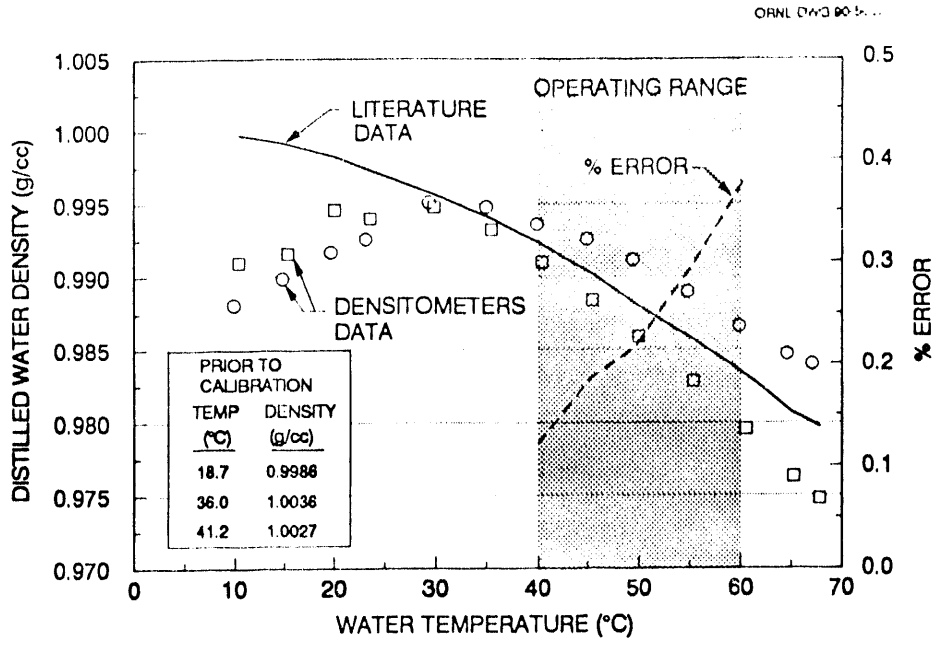

Fig. 3. TEMPERATURE CORRECTION APPLIED TO CORIOLIS FLOW METERS AND DENSITOMETERS.

where

m_{eq} = solution mass flow rate at film equilibrium point,
m_i = solution mass flow rate in the cup,
$m_{v\ abs}$ = vapor absorbed if subcooled,
$m_{v\ flash}$ = mass flashed if superheated.

Assuming adiabatic equilibration, an energy balance yields an expression for the mass flow rate of solution at the equilibrium point as follows:

$$\dot{m}_{eq} = \frac{\dot{m}_i(h_i - h_{fg}) - Q_w}{h_{eq} - h_{fg}} , \qquad (2)$$

where

Q_w = heat removed from the cooling water by flashing,
hfg_v = latent heat of water vapor,
h_i = enthalpy of solution entering the cup,
h_{eq} = enthalpy of solution in equilibrium with absorber pressure and temperature.

The algorithm initially guesses an equilibrium temperature (T_{eq}) and calculates an equilibrium concentration (C_{eq}) based on P, X, T thermodynamic relationships between T_{eq} and the absorber pressure (P_{abs}). A saturated solution enthalpy (h_{eq}) is calculated from C_{eq} and P_{abs} and is used in Eq. 2 to calculate the solution mass flow rate exiting the equilibrium point. The mass of solute, LiBr, remains constant during absorption, and a solute mass balance is used to calculate the exiting solution mass flow rate again based on a continuity balance of the solute as follows:

$$\dot{m}_{eq} = \dot{m}_i[\frac{X_i}{X_{eq}}] . \qquad (3)$$

The equilibrium temperature is incremented and iteration continues until the two calculations of exiting solution mass flow rate (Eqs. 2 and 3) converge. This calculated equilibrium temperature is used in calculating the log-mean-temperature and concentration differences. The absorber load, the heat transfer ($\dot{Q}$) from falling film to cooling water, was based on the water-side measurements. With knowledge of the load and the log-mean-temperature-difference, the average overall heat transfer coefficient was calculated by the following equations:

$$\dot{Q} = (UA)_o \Delta T_{lm} , \qquad (4)$$

$$\Delta T_{lm} = \frac{(T_{a_{eq}} - T_{c_o}) - (T_{a_o} - T_{c_i})}{\ln \frac{(T_{a_{eq}} - T_{c_o})}{(T_{a_o} - T_{c_i})}} , \qquad (5)$$

where

$(UA)_o$ = average overall heat transfer capacity,
ΔT_{lm} = log-mean-temperature-difference.

The average overall liquid-side mass-transfer coefficient is similar to the overall heat transfer coefficient. There is, however, an important difference in evaluation of the two coefficients. In heat transfer, the interfacial temperature is identical for each phase; but in mass transfer, there is a discontinuity in concentration at the liquid-gas interface. This occurs because in mass transfer, the driving potential within the phase is concentration. With knowledge of the mass of absorbate, based on a solute continuity balance, and the log-mean-concentration-difference, the average overall mass transfer coefficient was calculated by the following equations:

$$\bar{m}_v = K_L(\Delta c_{lm}) , \tag{6}$$

$$\Delta c_{lm} = \frac{c_e - c_{eq}}{\ln\left[\frac{(c_{if} - c_{eq})}{(c_{if} - c_e)}\right]} , \tag{7}$$

where

K_L = average overall liquid-side mass transfer coefficient,
Δc_{lm} = log-mean-concentration-difference,
c_{eq} = equilibrium concentration at absorber inlet,
c_{if} = interface concentration based on P_{abs} and T_{abs},
c_e = concentration exiting the absorber.

SELECTED ADVANCED SURFACES

Absorption theory for laminar LiBr-water films predicts that the thermal diffusion of the film will be two orders of magnitude greater than the mass diffusion; in other words, heat will be transferred readily across the solution film while mass (water vapor) absorbed at the film surface will tend to remain at the surface, thus inhibiting absorption of additional water vapor. Mixing of the film can enhance the absorption process, because the dominant concentration gradient occurs near the interface. Film mixing will induce secondary flows that reduce the diffusional resistance across the film and increase the mass transfer. The mixing can be achieved by tube surfaces that mechanically induce secondary flows in the solution film without increasing the mean film thickness. Several tube geometries were identified and tested to determine the possible enhancements achievable through film mixing. The advanced surfaces tested are shown in Fig. 4, along with the dimensional geometries, the fabrication processes, and the tube material.

Pin-fin Tube

The pin-fin surfaces were selected at the suggestion of DeVuono et al. (1990) and are commercially available. The pin-fin tubes had spine pitches of 6.4, 4.8, and 3.2 mm, respectively. Each tube had 26 fins per turn and the fin height was 3.2 mm. Flow visualization studies conducted in a bell jar at Battelle indicated that the fin pitch, longitudinal spacing between fin rows, caused mechanical mixing of the film and was by their estimate the most important geometric parameter to study. Testing proved this finding correct.

Twisted Tube

A proprietary twisted tube and a plain twisted tube having 4 starts per turn were tested. The plain twisted tube is commercially available; however, testing showed that the 45° helix angle of the tube was not suitable for absorption application. Solution would not remain on the tube and would literally sling off at various positions down the tube regardless of the solution flow rate. Attempts were made to wet the surface at high flow rates of about 0.025 kg/s and at low flow rates of about 0.003 kg/s. Solution would flow in rivulets down the tube and sling off the surface at several positions down the tube. Attempts were made to reduce surface tension and/or viscosity effects of the 60 wt% solution by heating the cooling water to about 50°C. After about 5 days of repeated failure, the plain twisted tube was judged inadequate for falling film application. The proprietary twisted tube did not incur the problems of the plain tube, and results follow of its performance compared with that of the other surfaces.

Fluted Tube

A fluted tube surface was also selected that was similar in geometry to the twisted tube. The helix angle of the flute was 22° with 24 starts per turn (i.e., lead length of 148 mm for each flute to make one revolution). The flute height and width at its base are 0.64 mm, and the flute was cut at a 60° angle to the normal of the tube surface. The fluted surface was suggested by Conlisk et al. (1987) as a good candidate surface that would be a limiting case for a twisted tube configuration. Dimensional geometry was gleaned from empirical analysis done by Conlisk et al. (1987).

Grooved Tube

A grooved tube surface having machined ridges of 1.5-mm height and spaced at 6-mm intervals was also tested. The dimensions for the grooved tube geometry were gleaned from the published work of Davies and Warner (1969), who experimentally determined the optimum surface roughness for promoting the gas absorption of CO_2 into distilled water running down an inclined plate. Davies showed the gas absorption to be fastest if the surface roughness induced wake interference type oscillations in the flowing water. Davies observed that as water flowed down over the ridges, vortices developed around each ridge. For a given groove separation and height, Davies observed the vortices to oscillate, giving the surface a flickering lattice-like appearance. If the groove spacing was too tight, the vortex shedding across the ridge was hindered;

- INTEGRAL FINS [illegible]
  FROM THE TUBING WALL ITSELF
- GEOMETRY: 26 FINS PER TURN,
  3.2 mm SPINE HEIGHT
  6.4 mm
  4.8 mm SPINE PITCH
  3.2 mm
  21.3 mm O.D. (UNDEFORMED)
  2.8 mm WALL
- MATERIAL: 304L STAINLESS STEEL

TWISTED TUBE SURFACE

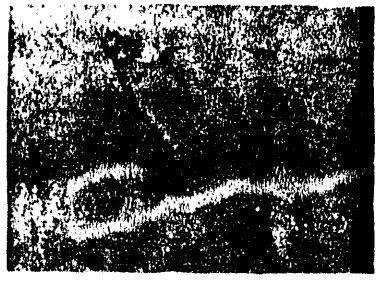

- TWISTING (STARTS) FORMED THROUGH EXTRUSION PROCESS
- GEOMETRY: 4 STARTS PER TURN
  45° HELIX ANGLE
  22.2 mm O.D. (UNDEFORMED)
  0.66 mm WALL
- MATERIAL: CARBON STEEL

FLUTED TUBE SURFACE

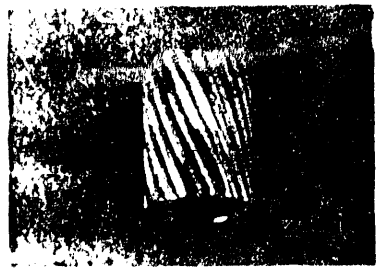

- FLUTES (STARTS) FORMED BY NUMERICALLY CONTROLLED MILLING MACHINE
- GEOMETRY: 24 STARTS PER TURN
  22° HELIX ANGLE
  0.64 mm FLUTE DEPTH
  19.1 mm O.D. (UNDEFORMED)
  2.4 mm WALL
- MATERIAL: 304L STAINLESS STEEL

GROOVED TUBE SURFACE

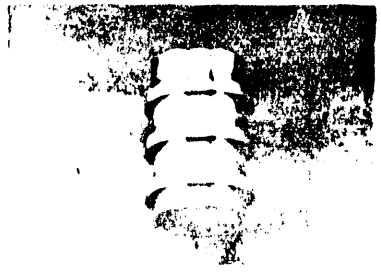

- GROOVES FORMED BY LATHE
- GEOMETRY: 19.1 mm O.D. (UNDEFORMED)
  6.4 mm PITCH
  1.5 mm KNURL HEIGHT
- MATERIAL: 304 L STAINLESS STEEL
- DESIGN GLEANED FROM WORK OF DAVIES, J.T. AND WARNER, R.K.V.

Fig. 4 ADVANCED SURFACES SELECTED FOR TESTING

conversely, if the spacing was too large, the vortex was less. In either case, gas absorption was reduced.

FALLING FILM VISUALIZATION

The hydrodynamics for smooth tube falling film flow are characterized as either laminar, wavy-laminar, roll-wave, or turbulent flows depending on the Reynolds number. Wavy-laminar and transitional roll-waves were observed during testing of the smooth tube for Reynolds numbers of about 150. Inception of the waves appeared to be affected by the solution flow rate. For testing at 0.011 kg/s, inception of short waves of small amplitude was observed 0.2 m down the tube; at 0.005 kg/s, inception was observed at 0.07 m. This short wave transitioned into a longer roll-wave whose length and amplitude were at least double that of the short wave. Similar observations were made by Brauner (1989), who characterized waves as a function of the film Reynolds number and downstream position. The wavy roll-wave flow was irregular or stochastic in nature. The larger roll-waves would flow over a thinner substrate of smaller waves. The wavelength of the roll-waves was of the order 0.05 m; at inception, the shorter waves were about 0.013 m. Wasden and Dukler (1990) presented similar findings and showed the falling film composed of small and large waves interacting in a complicated manner. Peak thickness was in many cases several times the mean.

The pin-fin and grooved tubes did an excellent job of mixing the falling film; however, the mixing mechanisms for the pin-fin and grooved tubes are very different. Both surfaces effectively enhanced performance. On the pin-fin tube with 6.4-mm pitch, a major flow could be seen falling in rivulets down the tube. The flow did not follow the spiral of the spines; rather, it flowed through the spines making one complete revolution over the length of the tube. No roll-wave phenomenon was observed flowing through the integral spines, and the film thickness in this flow was less than the fin height of 3.2 mm. Another less prominent flow could be seen flowing down along the base of the helical wrappings of the spines. Part of the flow would also drip from fin row to fin row, and was observed at about 0.3 m from the top and at about mid-section of the tube. The droplet flow probably increased the mass transfer of vapor into the falling film because of the droplet's high surface-to-volume ratio.

For the grooved tube, prominent roll waves traveled down the tube and the grooves broke up the waves, causing secondary flows that mixed the bulk of the film. Over the first 0.3 m of the tube, the roll waves traveled as a smooth wave with little disruption; then the ridges past 0.3 m would break up the waves into what appeared to be several little droplet streams still attached about the tube perimeter. These streams would then fall back into the falling film, probably because of the surface tension effects of the brine solution. Some droplets were observed to detach from the film; however, flow visualization studies showed this detachment to be very slight for falling film flows varying from 0.01 to 0.035 kg/s.

The axially fluted tube was observed to have the most uniform film of all the tubes tested. The fluting effectively channeled the flow and induced the falling film to flow both over and down the crests of the flutes. The spiraling motion increased the mean free-fall path of the falling film, which did enhance absorption slightly compared with a smooth tube. However, the flow appeared to have a strong tangential component of velocity, strong enough to make the falling film flow more wavy-laminar compared with the roll-wave laminar flow observed on the smooth and grooved tubes. The waves on the fluted surface were very regular with amplitudes of only about 25% of the roll-waves. As such, the strong tangential component of velocity caused by the flutes did not cause further mixing of the film compared with the grooved tube.

LABORATORY TEST RESULTS

Data for the advanced and smooth surfaces are listed in Table 1 for testing at 62 wt % LiBr brine, 10-mm Hg absorber pressure, and for cooling water controlled to 46°C flowing at 6.309×10^{-5} m³/s countercurrent to the falling film. The 10-mm Hg pressure translates into an evaporating temperature of about 12.8°C, which is representative of residential applications. Our original charter was to complement work conducted on the DEACH system (DeVuono et al. 1990). Therefore, the comparisons that follow are made for residential application with load rejection to a dry tower. However, the scope of testing was broadened to include commercial application also, and following residentially based comparisons, predictive comparisons based on empirical data are made to assess the performance of advanced surfaces vs that of a typical 200-ton single-stage chiller system.

Advanced Surfaces Test Results

Load comparisons of the pin-fin, grooved, proprietary twisted, fluted, and smooth tubes are shown in Fig. 5. The pin-fin tube having a pitch of 6.4 mm supported the largest load of all the tubes tested. Next were the grooved tube and the pin-fin tube with 4.8-mm pitch (not shown in Fig. 5), followed by the proprietary twisted tube. Performance of the fluted tube was of the same order as that of the smooth tube. The mass of water vapor absorbed followed similar trends and showed the enhancement factors of the pin-fin, grooved, and proprietary twisted tubes compared with the smooth tube. For the operating conditions listed in Fig. 6, the mass absorbed for the pin-fin tube was about double that observed for the smooth tube. For the grooved tube, the mass absorbed was slightly less than double that absorbed by the smooth tube. The twisted tube absorbed about 50% more than the smooth tube. Testing at 35°C cooling water showed similar improvements; however, the improvements were less than those observed at 46°C. The absorber load and the mass of vapor absorbed showed the pin-fin and the grooved tube to enhance performance by about 50% over that observed for the smooth tube.

The results for the pin-fin and grooved tubes show that the absorber load continues to increase as a function of solution flow rate (i.e., the more solution down the tube, the better its performance). Increasing the solution mass flow rate from

Table 1. VERTICAL-TUBE ABSORBER HEAT AND MASS TRANSFER DATA FOR TESTING AT 62 Wt % LiBr BRINE

		Pin-fin tubes			Grooved tube	Twisted tube	Fluted tube	Smooth tube
		6.4-mm	4.8-mm	3.2-mm				
P	mmHg	10.34	10.34	10.34	10.34	10.34	10.34	10.34
Re		144.1	143.8	138.6	170.0	132.6	175.9	216.9
Pr		22.3	22.8	23.4	22.5	22.3	22.1	22.2
Sc		2576.9	2664.2	2769.5	2620.7	2594.5	2555.3	2561.6
D_{AB}	m^2/s	$1.15x10^{-9}$	$1.14x10^{-9}$	$1.12x10^{-9}$	$1.14x10^{-9}$	$1.15x10^{-9}$	$1.15x10^{-9}$	$1.16x10^{-9}$
$T_{e_{eq}}$	°C	56.5	57.5	56.9	57.4	57.4	56.2	58.1
T_{e_o}	°C	51.7	49.0	49.5	50.6	48.6	50.4	52.4
$T_{e_{sc}}$	°C	2.7	6.4	6.0	3.9	6.3	4.0	3.5
T_{c_i}	°C	45.7	45.3	45.8	45.9	46.2	46.0	46.1
T_{e_o}	°C	49.3	48.5	48.1	48.7	48.7	47.9	48.3
T_{ABS}	°C	39.1	41.9	32.4	37.8	37.9	33.2	37.3
$\dot{m}_{e_i}$	kg/s	.012475	.012795	.012690	.011699	.012006	.013502	0.017017
$\dot{m}_e$	kg/s	.012658	.012977	.012811	.011934	.012215	.013654	0.017160
$\dot{m}_c$	kg/s	.0582	.0633	.0636	.0637	.0628	.0636	.0632
C_{eq}	g-mole/cc	$3.697x10^{-2}$	$3.667x10^{-2}$	$3.695x10^{-2}$	$3.676x10^{-2}$	$3.676x10^{-2}$	$3.715x10^{-2}$	$3.678x10^{-2}$
C_e	g-mole/cc	$3.746x10^{-2}$	$3.716x10^{-2}$	$3.727x10^{-2}$	$3.743x10^{-2}$	$3.734x10^{-2}$	$3.753x10^{-2}$	$3.707x10^{-2}$
$\dot{Q}$	W	878.4	839.0	624.7	756.8	669.0	502.9	578.6
K_L	m/s	$2.619x10^{-5}$	$2.869x10^{-5}$	$1.163x10^{-5}$	$3.814x10^{-5}$	$2.568x10^{-5}$	$1.769x10^{-5}$	$1.930x10^{-5}$
U	W/m^2-s	1302.6	1380.9	1033.2	1461.1	1583.9	897.3	799.6

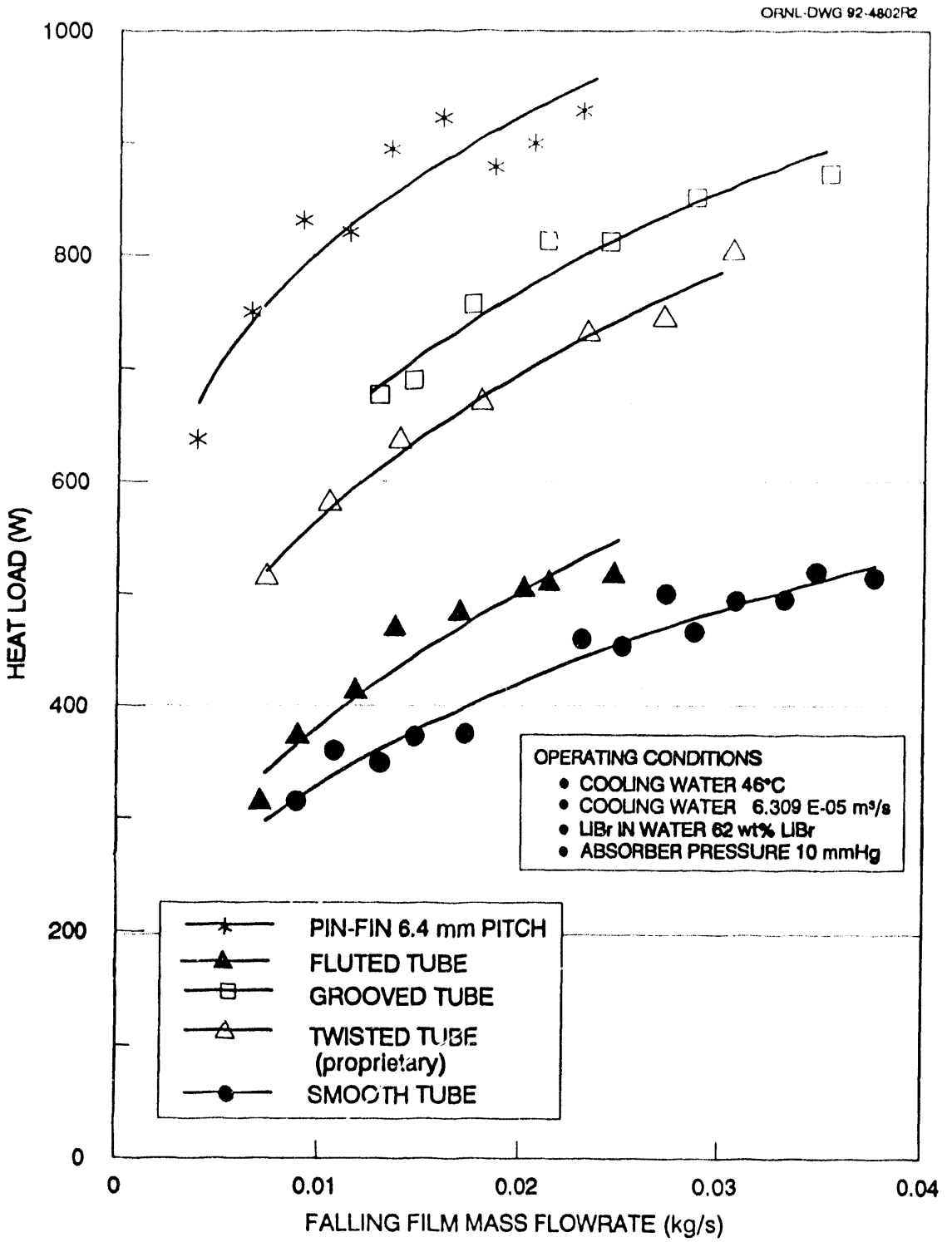

Fig. 5. THE HEAT LOAD FOR THE SMOOTH, PIN-FIN (6.4 mm PITCH), GROOVED, PROPRIETARY TWISTED, AND FLUTED TUBES.

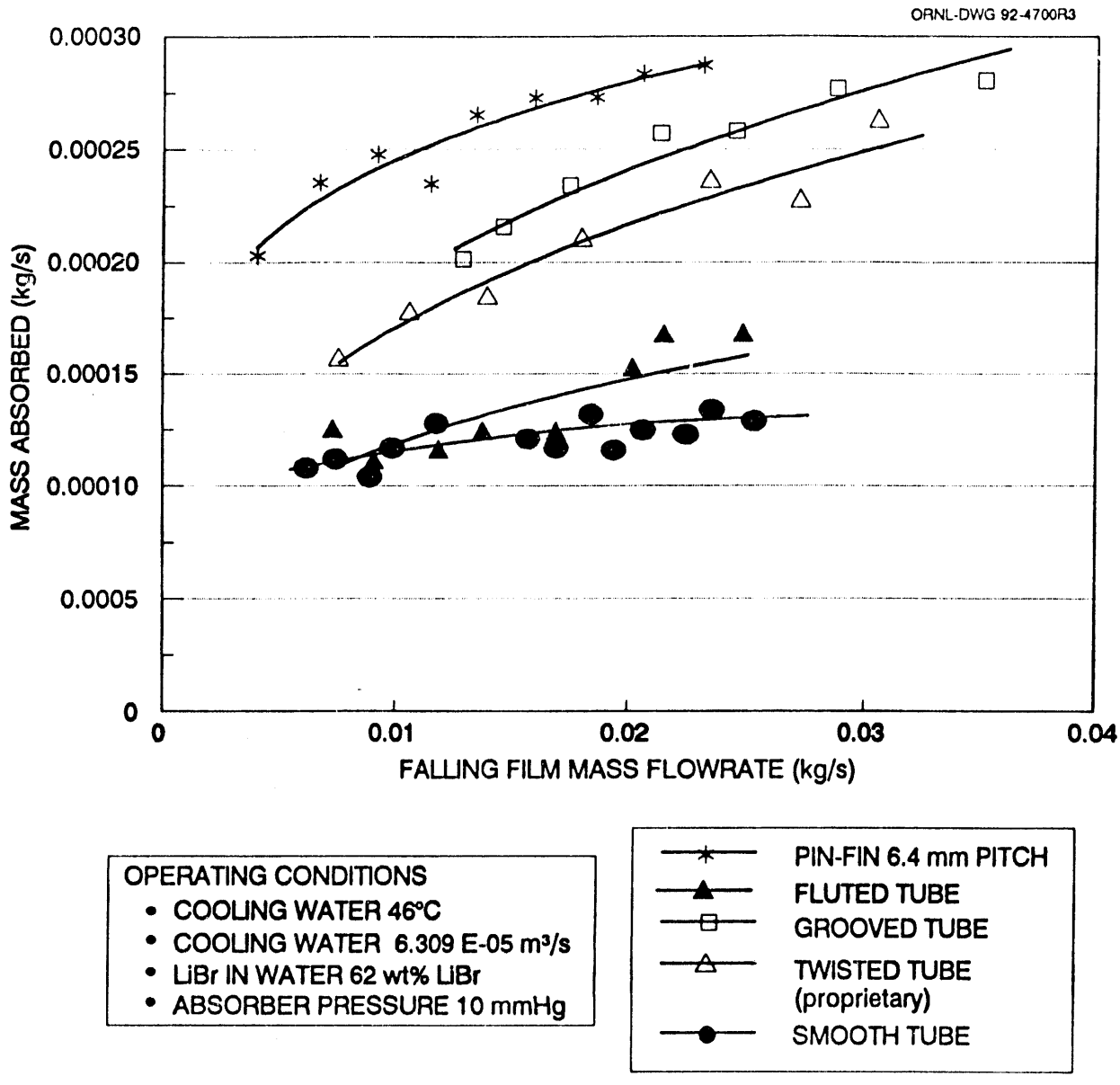

Fig. 6. THE RATE OF ABSORPTION FOR THE SMOOTH, PIN-FIN (6.4 mm PITCH), GROOVED, PROPRIETARY TWISTED, AND FLUTED TUBES.

0.01 to 0.03 caused about a 150% increase in capacity as caused by the increase in mass transfer. However, data showed the mass transfer to level off for the smooth tube for mass flow rates above 0.025 kg/s (Fig. 6).

Water temperature profiles for the smooth, pin-fin, and grooved tubes are shown in Fig. 7 for coolant inlet temperatures of 35 and 46°C, respectively. Film mixing on the advanced surfaces enhanced mass transfer and increased the temperature profile above that of the smooth tube. Fig. 7 shows the enhancement to occur over the entire length. In other words, the active lengths of the pin-fin and grooved tubes appear greater than that of the smooth tube as indicated by the level of subcooling leaving the respective tube surfaces. At a coolant inlet temperature of 46°C, the solution leaving the 6.4-mm pin-fin and the grooved tubes was about 2 to 3°C subcooled; at 35°C coolant temperature, the subcooling leaving these two advanced surfaces was 4 to 5°C, and the subcooling leaving the smooth tube was about 7°C.

Performance of the Pin-fin Tube

The absorber heat load for the tube with 6.4-mm pitch was about 50% greater than that of the 3.2-mm pitch tube for testing conducted at a concentration of 62 wt%, an inlet cooling water temperature of 46°C, and an absorber pressure of 10.3 mm Hg. Compared with the 4.8-mm pitch, the heat load for the 6.4-mm pitch was about 5 to 10% greater, indicating that an optimal pitch might be between 6 and 10 mm. The increase in heat load was due primarily to the increased mass flux to the spine fin surface (mass flux based on the outside diameter of the undeformed surface) (Fig. 8). Flow patterns for the tubes with 3.2- and 4.8-mm pitch did not show the dripping characteristic of the 6.4-mm pitch pin-fin tube, nor was any brine observed flowing down along the base of the spines. Visual observation revealed that for a given solution flow rate, the tighter pitch caused the film to thicken, possibly because of surface tension effects between the film and the spines. A thicker film indicates a higher interface temperature and a reduced pressure driving force, causing less mass transfer. Duplicate testing was conducted with a continuous purge to see if any hydrogen outgassing was affecting results for the tighter pitched tubes. Results showed similar absorber loads, within 5% of value with no purge active.

Performance of the Grooved Tube

Comparisons showed the grooved tube to be the second best performing absorption surface. For the grooved tube, the effect of increasing cooling water flow rate was observed to enhance performance significantly. In Fig. 9, test results at 6.309×10^{-5}, 1.262×10^{-4}, and 1.735×10^{-4} m³/s cooling water flow show the further increase in the mass absorbed. At 1.262×10^{-4} and 1.735×10^{-4} m³/s coolant flows and a falling film Reynolds number of about 150, absorption was enhanced by about 125% and 175%, respectively, of that observed at 6.309×10^{-5} m³/s. Increasing the cooling water flow reduced the heat transfer resistance from the cooling water to interface, which in turn dropped the interface temperature, causing an increase in absorption (Fig. 9). The optimal cooling water flow appears to be about 1.893×10^{-4} m³/s. This translates into an average velocity of about 1.5 m/s, which is close to the 2 m/s water velocity used in a 200-ton single-stage commercial chiller.

As previously stated for the smooth tube, increasing the falling film mass flow rate increases the film thickness, which in turn reduces the potential for mass transfer. However, the performance of the grooved tube continued to increase with increasing solution mass flow rate as seen in Fig. 9. The grooves induced secondary flows that mixed the bulk of the film and increased the pressure driving force for mass transfer. The overall mass transfer and heat transfer coefficients in Fig. 10 show that as the Reynolds number of the falling film increased, so did the mass transfer coefficient. This increase in overall mass transfer coefficient with increasing mass flow rate shows that the grooved tube increased the mass transfer without significantly affecting the film thickness. The heat transfer coefficient is shown in Fig. 10 to remain fairly constant with solution flow; increasing the cooling water flow rate did, however, enhance the overall heat transfer coefficient (Fig. 10).

LOADING COMPARISON: TEST RESULTS vs SINGLE-STAGE 200-TON CHILLER

A domestic single-stage 200-ton chiller would typically operate at 6.3 mm Hg absorber pressure, with 29.5°C cooling water flowing at about 0.593 kg/s per tube (i.e., 9.4 gpm per tube). LiBr brine would leave the boiler at about 64 wt % LiBr, but would enter the absorber at a concentration of about 62 wt % because of the chiller's recirculation design. The absorber has about 230 Cu tubes, each 0.019 m in outside diameter and 3.83 m in length. The chiller uses a chemical additive, 2-ethyl-1-hexanol at a concentration of about 500 ppm, to enhance performance.

Testing was not conducted at these identical conditions. However, testing was broadened to cover commercial applications; and data were collected for the 6.4-mm pitch pin-fin, grooved, and smooth tube surfaces at 7 and 8 mm Hg absorber pressures and for concentrations of 62 and 64 wt% LiBr. The empirical data were used to formulate and validate a model mathematically describing vertical-tube absorption (H. Perez-Blanco et al. 1993). Validation showed the model to predict absorber load and mass absorbed within about 20% of our laboratory values. Model output was then used to make a direct comparison with the performance of the 200-ton single-stage chiller system.

The evaporator flux for the described domestic chiller is about 13.3 kW/m² and is listed in Table 2, along with model predictions for the smooth, pin-fin, and grooved tubes. Predictions show that the pin-fin and grooved tubes yield nearly 80% and 70% higher evaporator flux, respectively, than the single-stage chiller. The level of subcooling is higher for the vertical vs the horizontal tube surfaces, probably because of the action of mechanical vs chemical mixing. The predictions do not account for the effects of noncondensables, nor the effect of pressure drop through an absorber tube bundle. Both of these

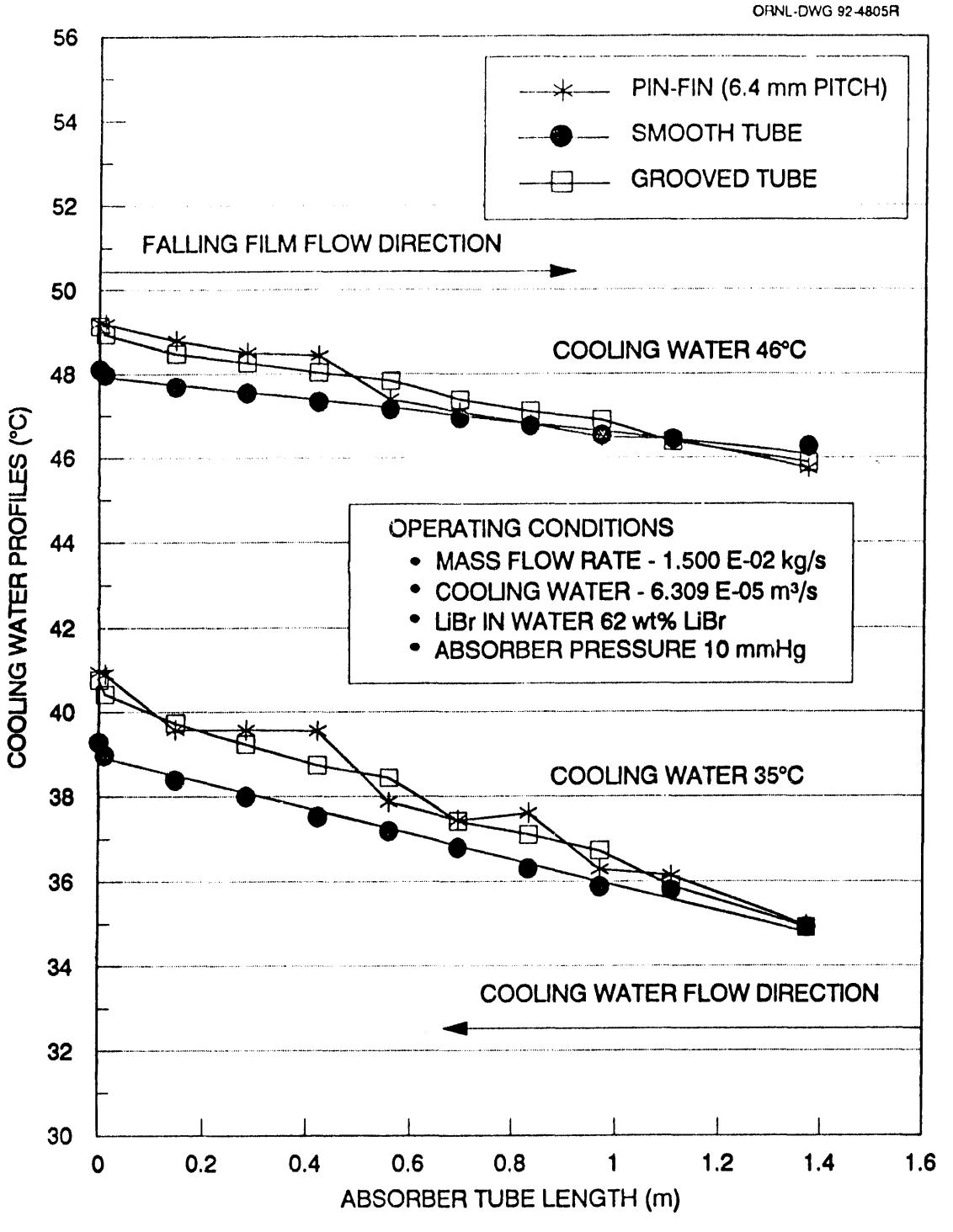

Fig. 7. COOLING WATER PROFILES FOR THE PIN-FIN (6.4 mm PITCH), GROOVED, AND SMOOTH TUBE

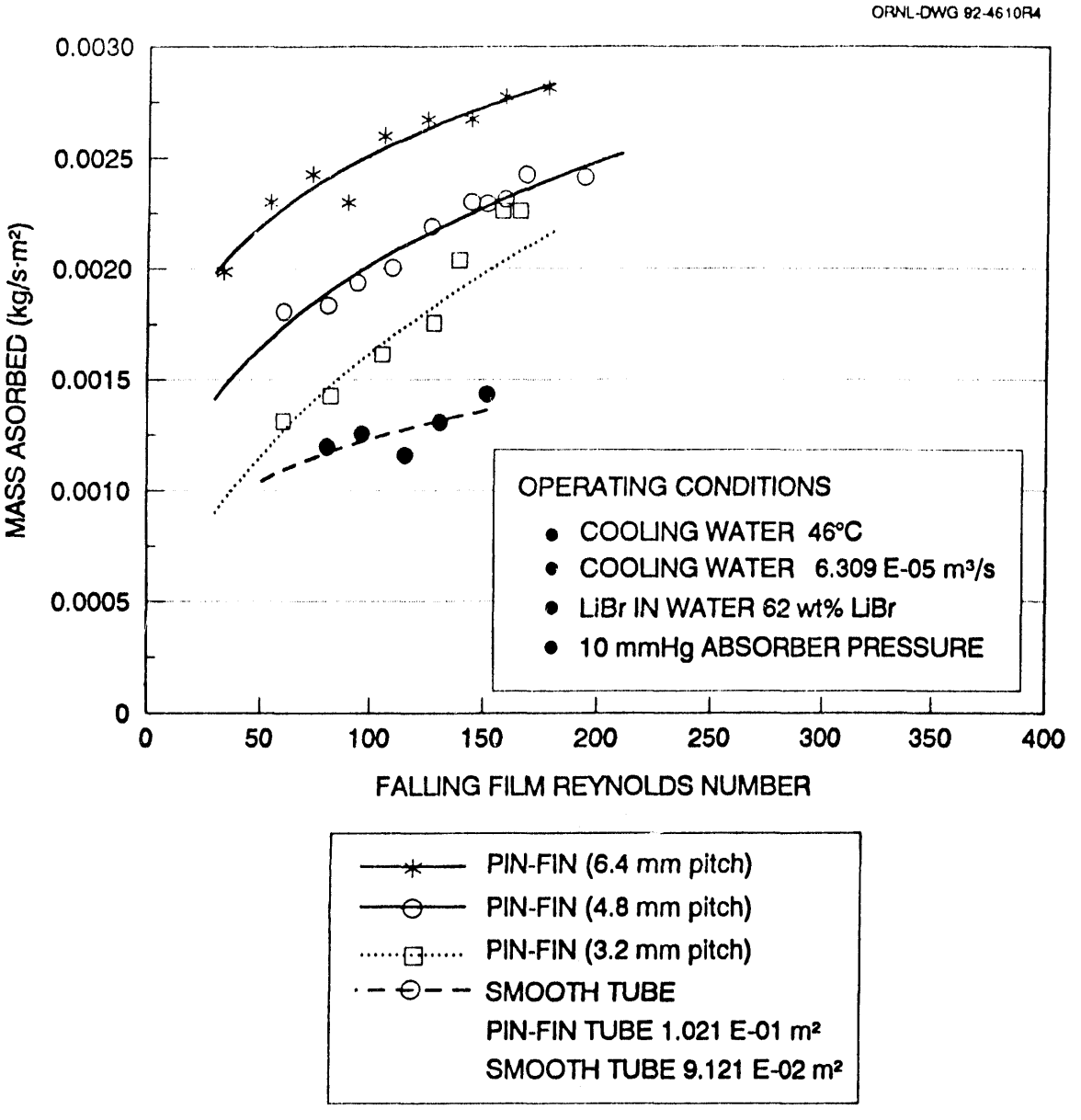

Fig. 8. COMPARISON OF MASS FLUX FOR THE PIN-FIN AND SMOOTH TUBE

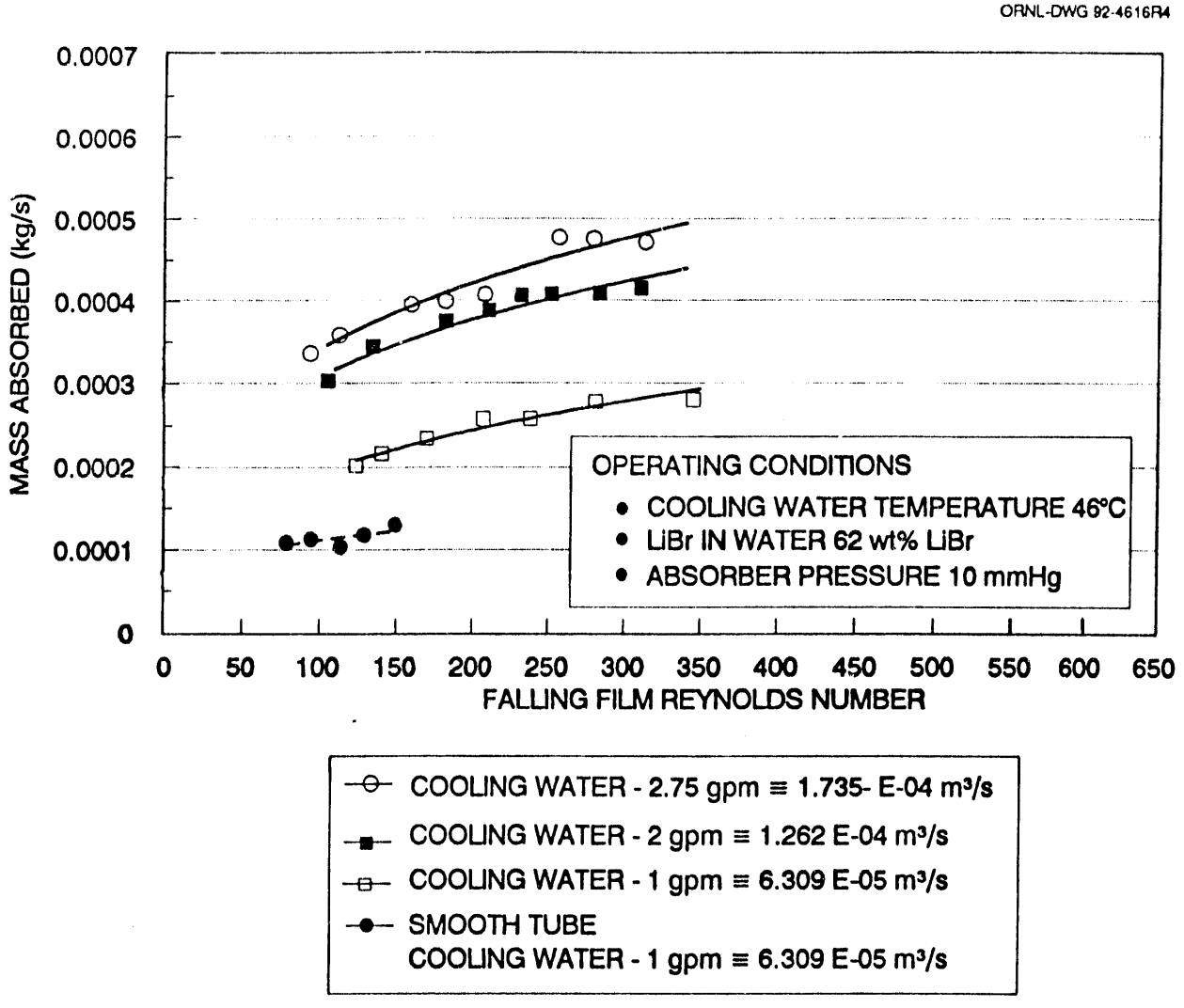

Fig. 9. ABSORPTION RATE FOR THE GROOVED TUBE FOR DIFFERENT COOLING WATER FLOW RATES.

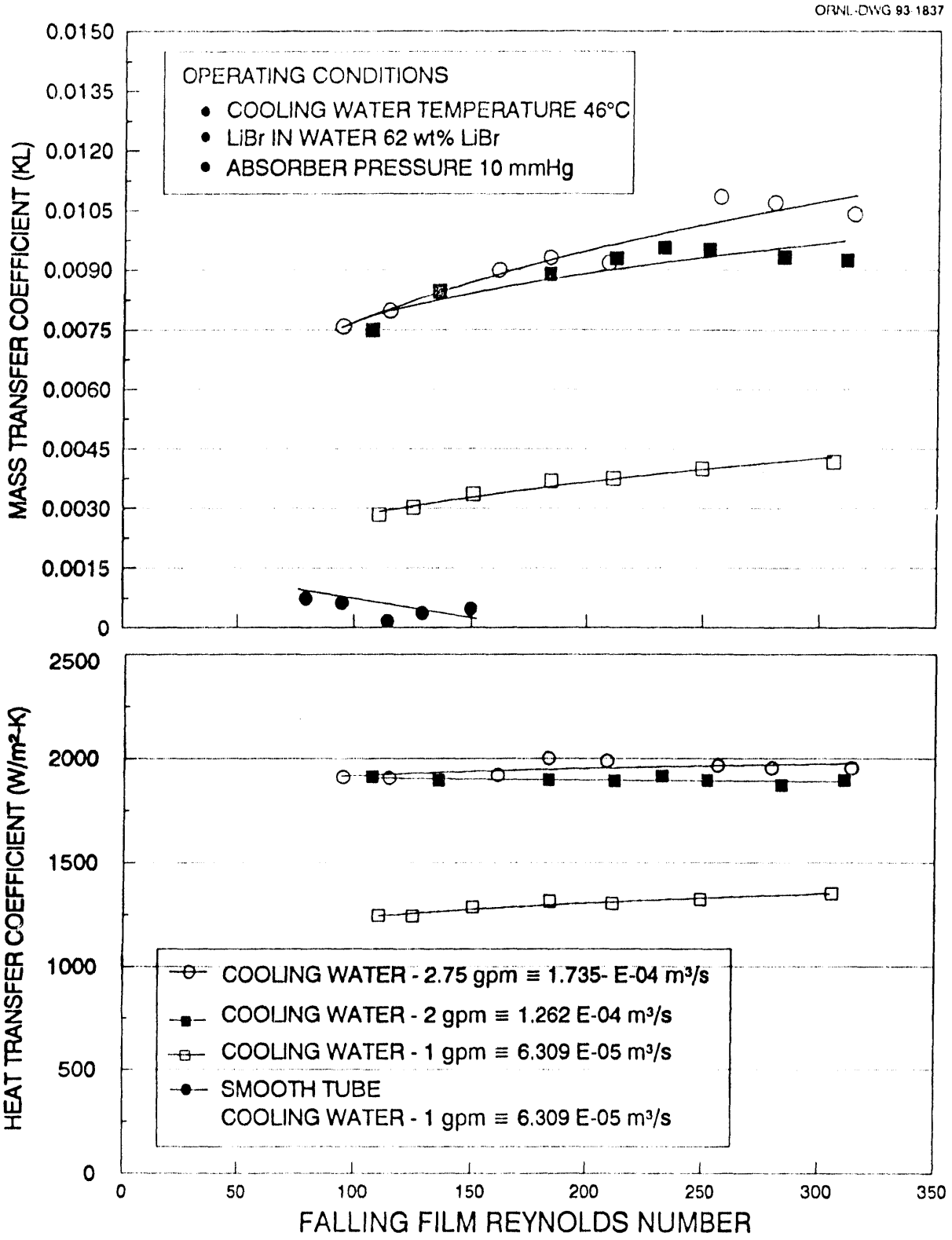

Fig. 10. TRANSPORT COEFFICIENTS FOR THE GROOVED AND SMOOTH TUBE.

Table 2. CALCULATED HEAT FLUX FOR VERTICAL-TUBE ABSORBER FOR COMPARISON WITH HORIZONTAL-TUBE COMMERCIAL 200-TON CHILLER

(X = 62 wt% LiBr, P_{abs} = 6.3 mmHg, Saturated
$\dot{m}_a$ = 0.03646 kg/s, $\dot{m}_c$ = 0.593 kg/s, T_{c_i} = 29.5°C)

	Evaporator flux (kW/m^2)	Subcooling (°C)
Model		
Smooth, roll-waves	10.1	13.0
Pin-fin, 6.4-mm pitch	22.8	9.6
Grooved	19.5	10.0
Commercial chiller		
200-ton single-stage	13.3	3.9–5.5

effects would reduce the performance improvements seen in Table 2 for the pin-fin and grooved tube surfaces. However, the results do show that the mechanical film mixing induced by these two surfaces may enhance absorption to levels comparable to that of chemical enhancement.

Cost becomes a significant factor for mechanical vs chemical enhancement. Advanced surfaces in single-stage equipment would not be cost effective. However, in applications such as high-temperature LiBr dual-stage systems, the use of advanced surfaces would eliminate the uncertainties of controlling chemical additive concentration in the system and the potential breakdown of the additive due to the higher operating temperatures of the system.

CONCLUSIONS

Testing was completed on smooth tube and advanced tube surfaces for LiBr brine concentrations of 60 through 64 wt%. The absorber pressure was set at 10 mm Hg, representing an 11°C evaporating temperature to complement work conducted on the DEACH residential system (DeVuono et al. 1990). Testing was also conducted at absorber pressures of about 7.8 mm Hg, representing a 7°C evaporating temperature, which is typical of commercial application. Water temperature was set to 35°C to simulate load rejection to a cooling tower, and to 46°C for load rejection to a dry coil.

Advanced surfaces were identified that enhanced absorber load and the mass of absorbate vapor. Test results prove that enhancement of the absorption process can be achieved by inducing a mixing in the solution film. Because the dominant concentration gradient occurs near the interface, film mixing induced secondary flows that reduced the diffusional resistance across the film and increased the mass transfer. Experiments and flow visualization helped to confirm this theory.

The pin-fin tube with 6.4-mm pitch increased the mass absorbed by about 225% over a smooth tube. A grooved tube was the second best performer with 175% enhancement over a smooth tube. A synergistic effect was achieved through an increase in the cooling water flow rate combined with the mechanical mixing occurring on the grooved tube. Performance was about 300% better than that of a smooth tube with the water flowing at 1.893×10^{-4} m^3/s.

Results indicate that absorbers made with either the pin-fin or grooved tubes would require fewer tubes and/or shorter lengths than absorbers made with smooth tubes. Thus, performance could be improved and both material and headroom space could be saved, yielding a more efficient and cost-effective absorber.

Results also show that both the pin-fin tube with 6.4-mm pitch and the grooved tubes potentially can enhance the absorption process to levels comparable to a single-stage commercially available chiller having horizontal smooth tubes with a chemical additive.

RECOMMENDATIONS

The pin-fin with 6.4-mm pitch would support a slightly larger evaporator capacity than would the grooved tube. An economic analysis is needed to show the cost effectiveness of the candidate surfaces. Also, system reliability would become an issue if the pin-fins were to break off and cause damage to the solution pumps.

It is recommended that further analysis be done on the pin-fin and grooved tubes to best optimize the surfaces for falling film absorption and to test them at higher operating

temperatures typical of prototype high-temperature LiBr dual-stage equipment. Results could yield a surface that enhances absorption by the same order as chemical enhancement, thus eliminating the problem of additive breakdown in high-temperature LiBr systems.

ACKNOWLEDGEMENTS

This work was sponsored by the Gas Research Institute. Its support and the program leadership of William A. Ryan, Gas Research Institute project manager, are gratefully acknowledged.

REFERENCES

Brauner, N., 1989, "Modeling of Wavy Flow in Turbulent Free Falling Films," *International Journal of Multiphase Flow*, Vol. 15, pp. 505-520.

Conlisk, A. T., and Johnson, R. E., 1987, "Laminar-film Condensation/Evaporation on a Vertically Fluted Surface," *Journal Fluid Mech.*, Vol. 184, pp. 245-266.

Davies, J. T., and Warner, K. V., 1969, "The Effect of Large-Scale Roughness in Promoting Gas Absorption," *Chemical Engineering Science*, Vol. 24, pp. 231-240.

DeVuono, A. C., Christensen, R. N., Lindstrom, D. K., Wilkinson, W. H., and Ryan, W. A., 1990, "Development of a Residential Gas-Fired Double-Effect Air Conditioner-HeaterUsing Water and Lithium Bromide," *ASHRAE Trans.*, Vol. 96, Pt. 1.

Patnaik, V., Perez-Blanco, H., and Ryan, W., 1993, "A Simple Model for the Design of Vertical Tube absorbers," *ASHRAE Trans.*, in press.

Wasden, F. K., and Dukler, A. E., 1990, "A Numerical study of Mass Transfer in Free Falling Wavy Films," *AIChE Journal*, Vol. 36, pp. 1379-1390.

Zaltash, A., Ally, M., Klatt, L. N., and Linkous, R. L., 1991, "Densities and Refractive Indexes of Aqueous (Li, K, Na)NO_3 Mixtures," *Journal of Chemical and Engineering Data*, Vol. 36, pp. 209-213.

Zaltash, A., and A., Ally, 1992, "Refractive Indexes of Aqueous LiBr Solutions," *Journal of Chemical and Engineering Data*, Vol. 37, pp. 110-113.

DATE

FILMED

1/6/94

END